Energy deposition from focused terawatt laser pulses in air undergoing multifilamentation

Guillaume Point, Emmanuelle Thouin, André Mysyrowicz, Aurélien Houard

Energy deposition from focused terawatt laser pulses in air undergoing multifilamentation

Guillaume Point,[1,2,*] **Emmanuelle Thouin,**[1] **André Mysyrowicz,**[1] **and Aurélien Houard**[1]

[1]*Laboratoire d'Optique Appliquée, ENSTA ParisTech, CNRS, Ecole Polytechnique, Université Paris-Saclay, 828 boulevard des Maréchaux, 91762 Palaiseau cedex, France*

[2]*ONERA-CP, Chemin de la Hunière et des Joncherettes, 91123 Palaiseau cedex, France*

[*]*guillaume.point@onera.fr*

Abstract: Laser filamentation is responsible for the deposition of a significant part of the laser pulse energy in the propagation medium. We found that using terawatt laser pulses and moderately strong focusing conditions in air, more than 60 % of the pulses energy is transferred to the medium, eventually degrading into heat. This results in a strong hydrodynamic reaction of air with the generation of shock waves and associated underdense channels for each of the generated multiple filaments. In the focal zone, where filaments are close to each other, these discrete channels eventually merge to form a single cylindrical low-density tube over a ~ 1 µs timescale. We measured the maximum lineic deposited energy to be more than $1\ \mathrm{J\cdot m^{-1}}$.

OCIS codes: (190.7110) Ultrafast nonlinear optics; (260.5950) Self-focusing; (350.5400) Plasmas.

References and links

1. A. Couairon and A. Mysyrowicz, "Femtosecond filamentation in transparent media," Phys. Rep. **441**, 47–189 (2007).
2. E. T. J. Nibbering, G. Grillon, M. A. Franco, B. S. Prade, and A. Mysyrowicz, "Determination of the inertial contribution to the nonlinear refractive index of air, n2, and o2 by use of unfocused high-intensity femtosecond laser pulses," J. Opt. Soc. Am. B **14**, 650–660 (1997).
3. T. Seideman, "On the dynamics of rotationally broad, spatially aligned wave packets," J. Chem. Phys. **115**, 5965–5973 (2001).
4. D. V. Kartashov, A. V. Kirsanov, A. M. Kiselev, A. N. Stepanov, N. N. Bochkarev, Y. N. Ponomarev, and B. A. Tikhomirov, "Nonlinear absorption of intense femtosecond laser radiation in air," Opt. Express **14**, 7552–7558 (2006).
5. S. Tzortzakis, B. Prade, M. Franco, and A. Mysyrowicz, "Time-evolution of the plasma channel at the trail of a self-guided IR femtosecond laser pulse in air," Opt. Commun. **181**, 123–127 (2000).
6. Y.-H. Chen, S. Varma, A. York, and H. M. Milchberg, "Single-shot, space- and time-resolved measurement of rotational wavepacket revivals in h2, d2, n2, o2, and n2o," Opt. Express **15**, 11341–11357 (2007).
7. Y.-H. Cheng, J. K. Wahlstrand, N. Jhajj, and H. M. Milchberg, "The effect of long timescale gas dynamics on femtosecond filamentation." Opt. Express **21**, 4740–4751 (2013).
8. G. Point, C. Milián, A. Couairon, A. Mysyrowicz, and A. Houard, "Generation of long-lived underdense channels using femtosecond filamentation in air," J. Phys. B: At. Mol. Opt. **48**, 094009 (2015).
9. N. Jhajj, E. W. Rosenthal, R. Birnbaum, J. K. Wahlstrand, and H. M. Milchberg, "Demonstration of long-lived high-power optical waveguides in air," Phys. Rev. X **4**, 011027 (2014).
10. O. Lahav, L. Levi, I. Orr, R. A. Nemirovsky, J. Nemirovsky, I. Kaminer, M. Segev, and O. Cohen, "Long-lived waveguides and sound-wave generation by laser filamentation," Phys. Rev. A **90**, 021801 (2014).

#256836 Received 11 Jan 2016; revised 1 Mar 2016; accepted 2 Mar 2016; published 11 Mar 2016

11. G. Dufour, B. Fornet, and F. Rogier, "Numerical modelling of supersonic flow actuated by laser-induced plasma," Int. J. Aerodynamics **3**, 122 (2013).
12. F. Vidal, D. Comtois, C.-Y. Chien, A. Desparois, B. La Fontaine, T. W. Johnston, J. Kieffer, H. P. Mercure, H. Pepin, and F. A. Rizk, "Modeling the triggering of streamers in air by ultrashort laser pulses," IEEE Trans. Plasma Sci. **28**, 418–433 (2000).
13. M. Mlejnek, M. Kolesik, J. V. Moloney, and E. M. Wright, "Optically turbulent femtosecond light guide in air," Phys. Rev. Lett. **83**, 2938–2941 (1999).
14. G. Fibich, S. Eisenmann, B. Ilan, Y. Erlich, M. Fraenkel, Z. Henis, A. Gaeta, and A. Zigler, "Self-focusing distance of very high power laser pulses," Opt. Express **13**, 5897–5903 (2005).
15. J. Yu, D. Mondelain, J. Kasparian, E. Salmon, S. Geffroy, C. Favre, V. Boutou, and J.-P. Wolf, "Sonographic probing of laser filaments in air," Appl. Opt. **42**, 7117–7120 (2003).
16. G. Point, "Energy deposition in air from femtosecond laser filamentation for the control of high voltage spark discharges," Ph.D. thesis, Ecole Polytechnique (2015).
17. A. Mermillod-Blondin, C. Mauclair, A. Rosenfeld, J. Bonse, I. V. Hertel, E. Audouard, and R. Stoian, "Size correction in ultrafast laser processing of fused silica by temporal pulse shaping," Appl. Phys. Lett. **93**, 021921 (2008).
18. Y. Brelet, A. Jarnac, J. Carbonnel, Y.-B. André, A. Mysyrowicz, A. Houard, D. Fattaccioli, R. Guillermin, and J.-P. Sessarego, "Underwater acoustic signals induced by intense ultrashort laser pulse," J. Acoust. Soc. Am. **137**, 288–292 (2015).
19. P. P. Kiran, S. Bagchi, C. L. Arnold, S. R. Krishnan, G. R. Kumar, and A. Couairon, "Filamentation without intensity clamping," Opt. Express **18**, 21504–21510 (2010).
20. G. Point, Y. Brelet, L. Arantchouk, J. Carbonnel, B. Prade, A. Mysyrowicz, and A. Houard, "Two-color interferometer for the study of laser filamentation triggered electric discharges in air," Rev. Sci. Instrum. **85**, 123101 (2014).
21. G. Point, Y. Brelet, A. Houard, V. Jukna, C. Milián, J. Carbonnel, Y. Liu, A. Couairon, and A. Mysyrowicz, "Superfilamentation in air," Phys. Rev. Lett. **112**, 223902 (2014).
22. E. W. Rosenthal, J. P. Palastro, N. Jhajj, S. Zahedpour, J. K. Wahlstrand, and H. M. Milchberg, "Sensitivity of propagation and energy deposition in femtosecond filamentation to the nonlinear refractive index," J. Phys. B: At. Mol. Opt. **48**, 094011 (2015).
23. F. Théberge, W. Liu, P. T. Simard, A. Becker, and S. L. Chin, "Plasma density inside a femtosecond laser filament in air: Strong dependence on external focusing," Phys. Rev. E **74**, 036406 (2006).
24. P. P. Kiran, S. Bagchi, S. R. Krishnan, C. L. Arnold, G. R. Kumar, and A. Couairon, "Focal dynamics of multiple filaments: Microscopic imaging and reconstruction," Phys. Rev. A **82**, 013805 (2010).
25. J. K. Wahlstrand, N. Jhajj, E. W. Rosenthal, S. Zahedpour, and H. M. Milchberg, "Direct imaging of the acoustic waves generated by femtosecond filaments in air," Opt. Lett. **39**, 1290 (2014).
26. K. Lim, M. Durand, M. Baudelet, and M. Richardson, "Transition from linear- to nonlinear-focusing regime in filamentation," Sci. Rep. **4**, 7217 (2014).

1. Introduction

Laser filamentation is a propagation regime for ultrashort laser pulses in transparent media reached when their peak power exceeds a critical power P_{cr}, which is about 5 GW in air at a wavelength of 800 nm. It results from a complex interplay between the optical Kerr effect, nonlinear energy absorption due to multiphoton and tunnel ionization and plasma defocusing [1]. While propagating in this regime, the laser pulse is able to maintain a high intensity over several Rayleigh lengths. Filamentation can deposit a significant part of the pulse energy in the propagation medium. Plasma generation itself, together with plasma absorption, form the main channel for energy deposition. Stimulated rotational Raman scattering on air molecules can also account for energy depletion of the laser pulse [2–4]. This energy, initially stored as potential and kinetic energy of plasma free electrons and as rotational energy of air molecules, is eventually converted into gas thermal energy after plasma recombination and rotational thermalization, occurring over $\sim$ 1 ns [5] and $\sim$ 100 ps timescales [6], respectively. The resulting heating can range from $\sim$ 100 K [7] to more than 1000 K [8], depending on experimental conditions. As air thermal conductivity is low, the system relaxes by launching an outward-propagating cylindrical pressure and density wave, expelling matter from the center of the channel and leaving a low-density tube. This underdense channel then slowly evolves by thermal diffusion, which can take times up to several tens of milliseconds [8]. Such laser-induced air hydrodynamics are

#256836 Received 11 Jan 2016; revised 1 Mar 2016; accepted 2 Mar 2016; published 11 Mar 2016

particularly interesting because they pave the way for the development of remotely generated, long-lived virtual optical structures such as optical waveguides [9, 10]. They could also be used in the prospect of enhanced aircraft aerodynamics [11]. As the efficiency of these structures is strongly dependent on the amplitude of laser-induced hydrodynamics effects, that is on local deposited energy, it is crucial to be able to increase the density of deposited energy at the required level.

In this Article, we study the influence of laser parameters on energy deposition. Surprisingly, despite the large amount of manuscript devoted to the study of filamentation in air by intense laser pulses, very few article report on the amount of laser energy transferred to the medium during this process [7, 12]. Thanks to a newly developed transverse interferometry technique we are able to determine energy deposition from multiterawatt laser pulses for the first time. We find that using the shortest and most energetic laser pulse with a moderately strong focusing, more than 60 % of the laser pulse energy is converted into heat at the terawatt peak power level. Since the laser pulse peak power is well above P_{cr} the beam forms many co-propagating filaments due to modulational instabilities [13, 14]. This results in the pulse energy being deposited in competing short-scale filaments instead of being concentrated in a single structure, which effectively limits the local energy deposition. Investigating the air hydrodynamics response by means of transverse interferometry, we witnessed a spontaneous evolution of the system from discrete underdense channels to a cylindrically-symmetric form with a single, large channel and an associated unique shock wave, partially negating the deleterious effect of multifilamentation. In optimal conditions, this channel lasts for more than 100 ms. Using a sonographic technique [15, 16], we estimated the peak lineic deposited energy to be $1.3\,\mathrm{J}\cdot\mathrm{m}^{-1}$.

2. Optimizing energy deposition

We first determined optimal experimental conditions to get the maximum absolute energy deposition from filamentation. To this purpose, we used a direct measurement of the laser pulse energy right after the focusing lens and ~ 10 cm after the end of the laser-induced plasma by means of a Joule meter (model QE50LP-H-MP from Gentec-EO). The difference between input and output energy was considered as deposited energy, which is a good approximation since energy losses due to Rayleigh and Thomson scattering are negligible. Such measurements were repeatedly done while varying laser pulse energy, laser pulse duration and focusing conditions.

2.1. Laser pulse energy

The first investigated laser parameter was laser pulse energy. For this study a moderately strong focusing at $f/30$, corresponding to a 100 cm focal length, was used with a 50 fs laser pulse at 800 nm. In these focusing conditions, laser pulse propagation is lens-dominated, with a minor contribution coming from the Kerr effect [26]. Evolution of deposited energy with input energy is displayed in Fig. 1.

In this figure are plotted two curves: first, the total deposited energy (red circles), that is the difference between input and output energies and second, the relative deposited energy (blue squares), that is deposited energy normalized by input energy. The global trend is an increase of deposited energy with input energy. Deposited energy evolves quasi linearly at higher laser energies. As for relative deposited energy, it can roughly be divided in two parts: the first one, up to $E_{in} \approx 20$ mJ, is characterized by a very steep increase, reaching up to 35 %. Past this point, relative deposited energy still increases, but much more slowly, and eventually saturates around 60 % beyond $E_{in} \approx 110$ mJ. We attribute the transition observed around 20 mJ, that is a peak power of about $80P_{cr}$, to the threshold described by Fibich and co-authors between, on the one hand, a full beam self-focusing, yielding the formation of a single filament at the nonlinear focus, and, on the other hand the breaking-up of the beam in multifilaments before the nonlinear

#256836 Received 11 Jan 2016; revised 1 Mar 2016; accepted 2 Mar 2016; published 11 Mar 2016

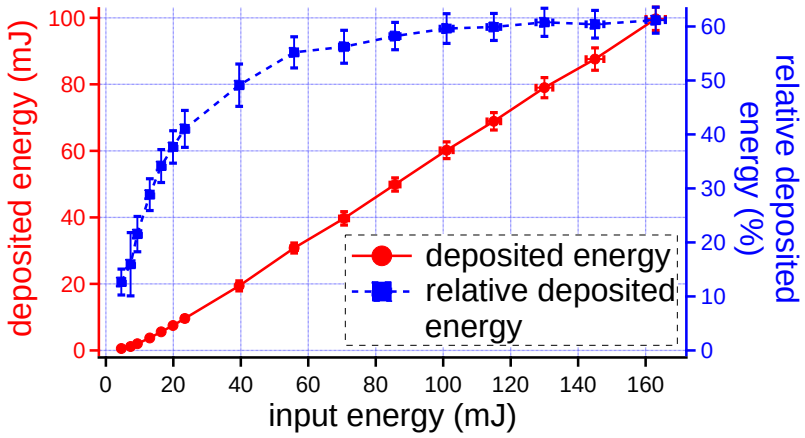

Fig. 1. Evolution of the total (red circles) and relative (blue squares) deposited energy with input energy from the filamentation of a 50 fs laser pulse at 800 nm focused at $f/30$. Error bars correspond to a confidence interval of one standard deviation evaluated over 500 shots.

focus [14]. This means that as soon as the beam breaks up into short-scale filaments before the focal zone, where the majority of energy deposition occurs, increasing input energy leads to a redistribution of this energy over many competing filaments, only slightly increasing deposited energy for each of them.

2.2. *Laser pulse duration*

Influence of the laser pulse duration on energy deposition was investigated by fixing input energy and focusing conditions and by detuning the laser compressor, imparting temporal chirp to the pulse.

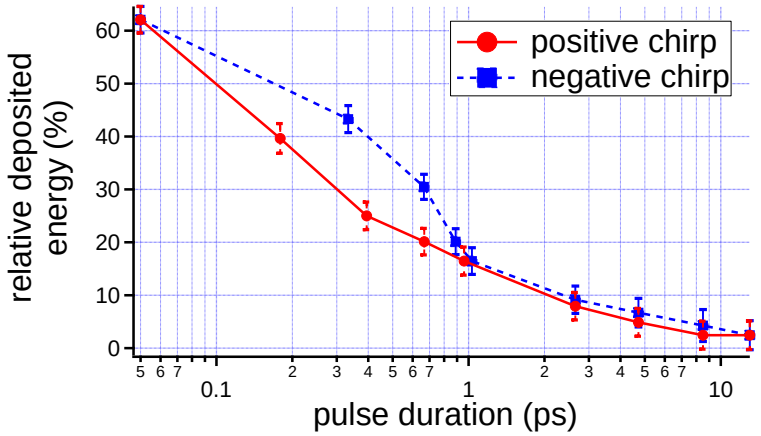

Fig. 2. Evolution of the relative deposited energy with pulse duration in the case of positive (red circles) and negative chirp (blue squares). Filamentation was generated by a 164 mJ laser pulse at 800 nm focused at $f/30$. Error bars correspond to a confidence interval of one standard deviation evaluated over 500 shots.

#256836 Received 11 Jan 2016; revised 1 Mar 2016; accepted 2 Mar 2016; published 11 Mar 2016

Results displayed in Fig. 2 are unambiguous: pulse duration is a very sensitive parameter. As soon as it deviates from the minimum value of 50 fs, that is from a maximum peak power, deposited energy quickly falls, being reduced from more than 60 % to less than 20 % at 1 ps, and to only a few percents past 10 ps. It is worth mentioning that a negative chirp yields better results than a positive chirp. This can be explained by the plasma defocusing effect affecting the back of the pulse, which is stronger at longer wavelengths and will therefore tend to decrease the intensity of positively chirped pulses more than for negatively chirped pulses.

One could think that as some energy transfer channels, like avalanche ionization, are favored by longer pulses, it could positively affect energy deposition. Such behavior has indeed been observed during filamentation in fused silica [17] and water [18]. Conversely, it seems that maximum intensity gives the best results in air, because it promotes a more efficient nonlinear ionization and Raman absorption, in the limit of pulse durations that can be achieved with our laser system.

2.3. Focusing conditions

Influence of focusing conditions was also studied by comparing three cases: a moderate focusing at $f/60$, a stronger focusing at $f/30$ and an extreme focusing at $f/3$, corresponding to the quasi-breakdown regime described by Kiran *et al.* [19]. All these cases are lens-dominated, with the Kerr effect playing only a marginal role in the formation of filaments [26]. Results are given in Fig. 3. It shows that for a given input energy, energy deposition is maximum in the $f/30$ case. The three cases also exhibit a regime transition around 20 mJ, which is more obvious for weaker focusing, with a first phase where energy deposition quickly increases followed by a second phase where it rises slowly or stagnates.

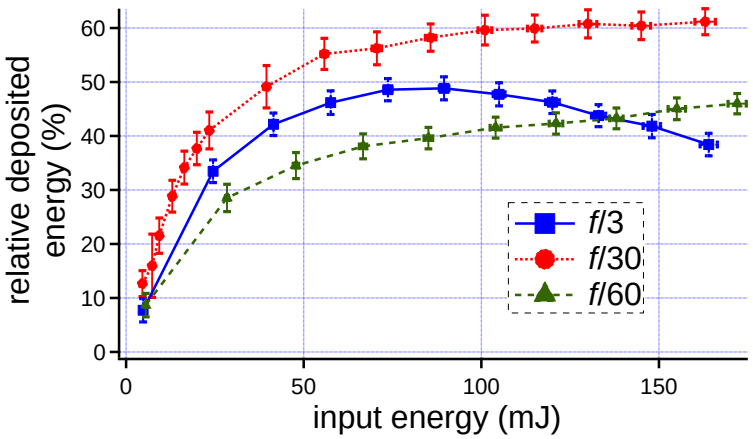

Fig. 3. Evolution of the relative deposited energy with input energy using a $f/3$ (blue squares), a $f/30$ (red circles) or a $f/60$ focusing (green triangles). Filamentation was generated by a 50 fs laser pulse at 800 nm. Error bars correspond to a confidence interval of one standard deviation evaluated over 500 shots.

Interesting features observed with the strong $f/3$ focusing are that deposited energy is significantly lower than in the $f/30$ case and that relative energy deposition reaches a maximum around 85 mJ at ~ 50 % and then starts to slowly decrease, going below 40 % at 165 mJ. This behavior might be explained by the fact that such a strong focusing promotes the generation of a very dense and short plasma with an accordingly strong defocusing effect, leading to a de-

#256836 Received 11 Jan 2016; revised 1 Mar 2016; accepted 2 Mar 2016; published 11 Mar 2016

crease of intensity and therefore to a less efficient energy deposition. Even though this decrease is modest, it results in energy deposition with $f/3$ focusing to be lower than energy deposition in the $f/60$ case at high input energy.

3. Energy deposition in the high energy limit

3.1. Filamentation-generated hydrodynamics

We then concentrated on the case that yielded the most important energy deposition: a 165 mJ, 50 fs (3.3 TW) laser pulse at 800 nm focused at $f/30$. To characterize filamentation-induced hydrodynamics, we performed transverse interferometry on laser-generated air channels using the same instrument presented in references [8], [16] and [20]. In this pump-probe experiment, a filament is first generated in one of the arms of a Mach-Zehnder interferometer. A probe pulse from a triggered Nd:YAG laser then enters the interferometer and intercepts filamentation-induced air structures transversely, allowing the reconstruction of the corresponding two-dimensional refractive index profile by means of the inverse Abel transform at the condition that this profile has a cylindrical symmetry.

As a large number of multifilaments is generated and, therefore, the laser beam exhibits a strong inhomogeneity, we did not expect the system to have a cylindrical symmetry, preventing us to use the Abel inversion to retrieve air density radial profiles. Nevertheless it was found that in the focal zone after a given delay, air density spontaneously evolves from a highly disorganized state, reminiscent of multifilamentation, to a cylindrically-symmetric state, as displayed in Fig. 4(a). In this last figure are plotted two line-integrated air density profiles taken at the linear focus. At delay 200 ns, several structures can be seen at the center of the profile, undoubtedly resulting from discrete short-scale filaments. The picture is very different at delay 500 ns because at this time, line-integrated density turned into a much more organized state with a good symmetry.

Since the system becomes cylindrically-symmetric after some time, Abel inversion can be used to compute air density profiles. Results are displayed in Fig. 4(b). These profiles are characterized by an outward-propagating cylindrical shock wave leaving a central underdense channel, much in the same way as single filamentation. In the present case however, the shock is broader and its amplitude is higher than in the case of high-energy monofilaments (see results given in reference [8] for comparison), while the underdense channel has approximately the same depth at about 30 % of normal air density, but is significantly larger, reaching a full width at half maximum of 2 mm after 10 μs. We still recorded the presence of the density hole after 100 ms, the maximum time we could reach due to experimental constraints. By this time, it enlarged so much that it affected the whole field of view of the camera, preventing us from extracting air density. Shock speed u_{SW} was evaluated using shock radial position r_{SW} and is plotted in Fig. 4(c). It exhibits a steep initial increase up to $\sim 500\,\mathrm{m\cdot s^{-1}}$ during the first microsecond, followed by a slower, gentle decrease at subsequent times, still propagating with a supersonic speed after 10 μs.

The symmetrization process is highly dependent on the position along the filament bundle and, therefore, on the local profile of energy deposition. For instance, looking at the time evolution of line-integrated air density at position $z = 96$ cm [Fig. 5], we see that in this case, symmetrization takes a much longer time than at $z = 1$ m and remains incomplete even after 10 μs, but still occurs by 100 μs. This gives a clue about the origin of symmetrization. We explain it as follows: multifilamentation results in an inhomogeneous energy deposition, which occurs in several separated channels. Each filament forms a hydrodynamic wave and the associated air underdense channel. If filaments are initially close enough one from the other, as it is the case in the focal zone, individual shock waves quickly interfere constructively, leading to the formation of a single, large shock wave, much in the same way it was observed by Wahlstrand and

#256836 Received 11 Jan 2016; revised 1 Mar 2016; accepted 2 Mar 2016; published 11 Mar 2016

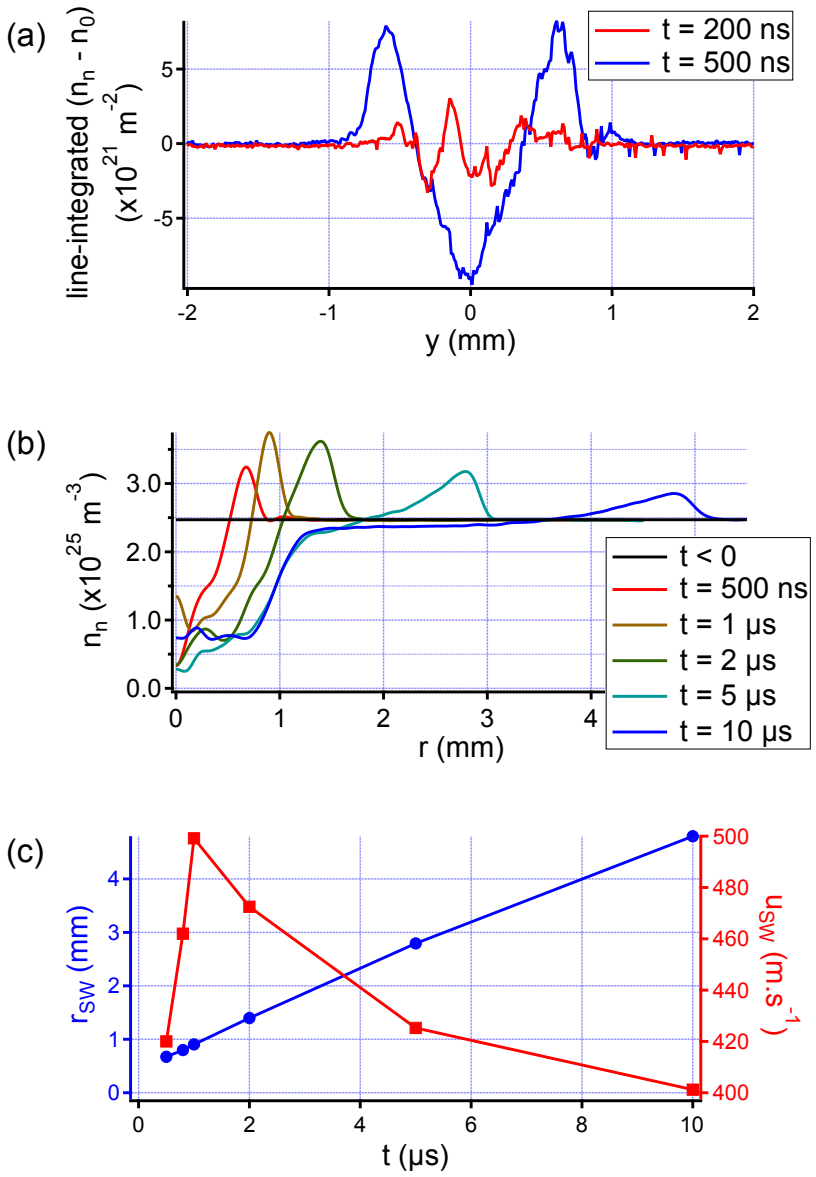

Fig. 4. (a): line-integrated air density profiles at $z = 1$ m after the focusing lens (linear focus) for two different delays, displaying self-symmetrization. (b): radial air density profiles extracted after channel symmetrization at $z = 1$ m. (c): evolution of the shock wave radius r_{SW} (blue circles) and shock wave speed u_{SW} (red squares). Filamentation was generated by a 165 mJ, 50 fs laser pulse at 800 nm focused at $f/30$.

co-authors with filament structures from a LG_{04} beam [25]. The time interval during which u_{SW} increases [Fig. 4(c)] can be seen as a sign of this interference process during which the fastest components from the strongest filaments catch up with the slowest components and eventually take the lead. Since in the focal zone at this energy level and with these focusing conditions the laser pulse propagates in the *superfilamentation* regime [21], plasma and therefore energy de-

#256836 Received 11 Jan 2016; revised 1 Mar 2016; accepted 2 Mar 2016; published 11 Mar 2016

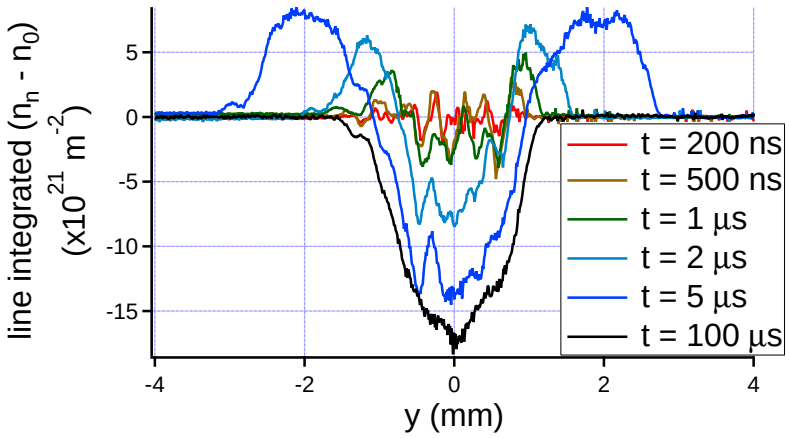

Fig. 5. Line-integrated air density profiles recorded at $z = 0.96$ m after the focusing lens and for different times. Filamentation was generated by a 165 mJ, 50 fs laser pulse at 800 nm focused at $f/30$.

position profile are distributed in a much more symmetric fashion than in standard short-scale filamentation areas. This explains why the shock exhibits an almost perfect cylindrical symmetry since it originates from the deposited energy spatial profile. As the shock is responsible for the generation of the underdense channel by ejecting matter from the center, a symmetric shock means that the associated underdense channel will also be symmetric, as observed here. When symmetrization is only partial once the shock has left (as displayed in Fig. 5), thermal diffusion can act over longer timescales to smooth out any remaining sharp density features, yielding a *diffusive* symmetrization, unlike the pure *acoustic* symmetrization process occurring near the linear focus.

3.2. *Lineic deposited energy*

Still investigating the case of a 165 mJ, 50 fs laser pulse focused at $f/30$, we estimated the lineic deposited energy using a sonographic technique. It consists in scanning the acoustic emission from the filament bundle along the laser propagation direction by means of a microphone (model 4138 from Brüel & Kjaer) [15, 16]. Indeed, since heating due to filamentation occurs much more quickly than the characteristic development time of air hydrodynamic response, we can consider it as an isochoric process. If we write the deposited energy as ΔU then the first law of thermodynamics reads:

$$\begin{aligned}\Delta U &= c_v n_0 \int_{\mathbb{R}^3} (T(\vec{r}) - T_{air})\, \mathrm{d}^3\vec{r} \\ &= \frac{c_v}{k_B} \int_{\mathbb{R}^3} (p(\vec{r}) - p_{air})\, \mathrm{d}^3\vec{r}, \end{aligned} \tag{1}$$

where c_v is the isochoric heat capacity of an air molecule and $n_0 = 2.47 \times 10^{25}$ m^{-3} is the air density at $p_{air} = 1.013 \times 10^5$ Pa and $T_{air} = 300$ K. In the case of an initial pressure profile with cylindrical symmetry, this equation can be simplified as:

$$\Delta U \approx \frac{\pi c_v}{k_B} \int_{\mathbb{R}} (p_{max}(z) - p_{air}) r_0(z)^2\, \mathrm{d}z, \tag{2}$$

#256836 Received 11 Jan 2016; revised 1 Mar 2016; accepted 2 Mar 2016; published 11 Mar 2016

where $r_0(z)$ is the half width at half maximum (HWHM) of the temperature profile at z. Assuming that r_0 does not vary significantly along the acoustic source, we find:

$$\Delta U \propto \int_{\mathbb{R}} (p_{max}(z) - p_{air})\, \mathrm{d}z. \tag{3}$$

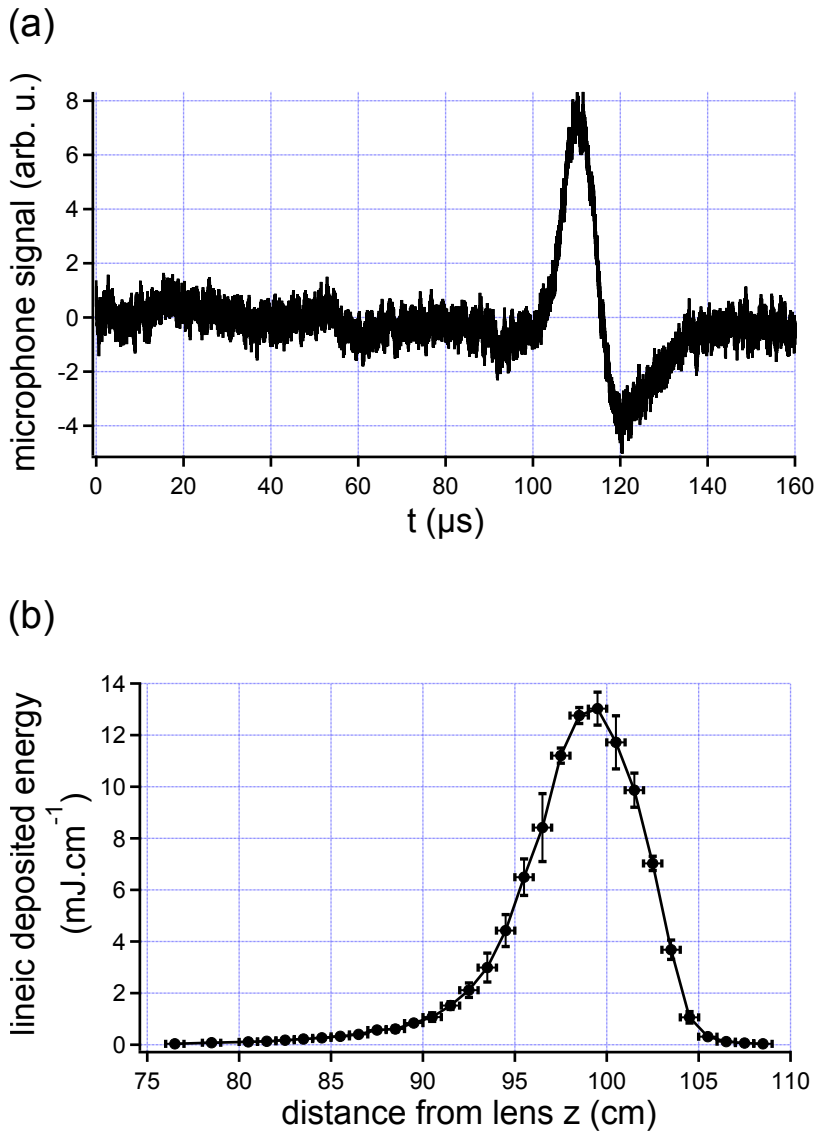

Fig. 6. (a): example of microphone signal recorded at $z = 80$ cm and 30 mm away from the laser beam center, displaying only a single large overpressure peak followed by a longer underpressure phase. (b): spatial evolution of the lineic deposited energy from a 165 mJ, 50 fs laser pulse at 800 nm focused at $f/30$. This curve was obtained from sonographic measurements of the bundle acoustic emission and by equating the z-integral of the corresponding scan with total deposited energy. Error bars correspond to a confidence interval of one standard deviation evaluated over 200 shots.

#256836 Received 11 Jan 2016; revised 1 Mar 2016; accepted 2 Mar 2016; published 11 Mar 2016

According to this last equation, the z-evolution of the peak pressure recorded with a microphone in the case of an initially cylindrically-symmetric pressure profile gives the envelope of the lineic deposited energy along z. One can then equate the integral of this curve with the total deposited energy, as recorded by a Joule meter like in the previous section, to get the absolute lineic deposited energy curve.

If this method works well in the case of a single filament [22], it cannot be directly applied in the present case because the initial pressure profile is not cylindrically symmetric, preventing us from using the approximation of Eq. (2). The symmetrization process in the focal zone can be used at our advantage. As the system spontaneously evolve to this cylindrically-symmetric state, we can consider it as if it started from a cylindrical pressure profile with a similar initial energy. We then make the assumption that most of energy deposition occurs around the focal zone where this effect is at its strongest, enabling us to retrieve the lineic deposited energy following Eq. (3).

As seen in Fig. 6(a), the filament bundle already generates a single acoustic wave as far as 20 cm away from the linear focus, showing that at least a partial acoustic symmetrization occurs at this position and strengthening our hypothesis. We therefore performed a full acoustic scan along the filament bundle and equated the integral of the corresponding curve with deposited energy following Eq. (3). Results are plotted in Fig. 6(b). They exhibit a zone about 15 cm long where lineic deposited energy is above 1 $\mathrm{mJ\cdot cm^{-1}}$, reaching a peak value of 13 $\mathrm{mJ\cdot cm^{-1}}$ shortly before the linear focus, confirming that most of the energy deposition takes place in the focal zone. As a comparison, high-energy single filamentation presented in reference [8] only reached a 400 $\mathrm{\mu J\cdot cm^{-1}}$ maximum energy deposition.

3.3. Physical investigation of energy deposition

Investigating the underlying physics of laser energy deposition asks for a good knowledge of the different vectors for energy absorption. Plasma generation is the easiest one to characterize. To this purpose we used a spectroscopic analysis of the plasma luminescence. It was shown previously by Théberge *et al.* that emission from the first negative system of the N_2^+ cation can be used as a plasma diagnostic following:

$$\int_{\mathbb{R}} L(z)\,\mathrm{d}z \propto N_e, \tag{4}$$

where L is the luminescence signal at position z along the multifilament bundle and N_e the total number of free electrons in the plasma [23].

This means that plasma luminescence from the first negative system of N_2^+ is proportional to the area-integrated electron density:

$$L(z) \propto \int_{\mathbb{R}^2} n_e(r,\theta,z) r\,\mathrm{d}r\mathrm{d}\theta. \tag{5}$$

We recorded plasma luminescence along the multifilament bundle at wavelength 391 nm using a monochromator (model H-20 from Jobin Yvon) with a $\sim$ 1.5 nm spectral resolution. Results are plotted in Fig. 7, compared with the lineic deposited energy profile.

From this figure, one can see that the total plasma length is in excess of 15 cm, starting slightly before $z = 90$ cm and ending between $z = 105$ and $z = 110$ cm. It is interesting to note that energy deposition clearly starts increasing before plasma luminescence, indicating that in the area before the focus ionization alone is not the main channel for energy deposition. This behavior can be explained by the stimulated rotational Raman scattering of the laser on air molecules [3]. Also, ionization of O_2 starts before that of N_2 because of a lower ionization potential and can deplete the laser energy while not yielding any luminescence from excited N_2^+.

#256836 Received 11 Jan 2016; revised 1 Mar 2016; accepted 2 Mar 2016; published 11 Mar 2016

Conversely, once in the focal zone, lineic deposited energy and plasma luminescence behave quite similarly, decreasing simultaneously and almost completely disappearing past $z = 105$ cm. This good agreement shows ionization becomes the main channel for energy deposition close to the focus.

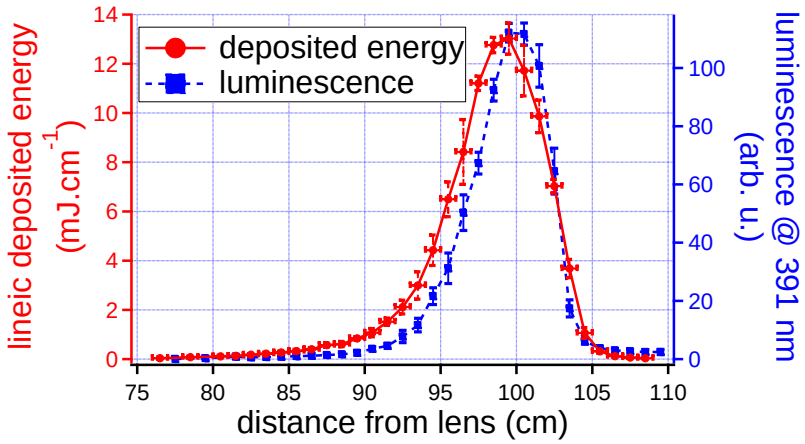

Fig. 7. Plasma luminescence from the first negative system of N_2^+ at 391 nm (blue squares) and lineic energy deposition profile (red circles) along the multifilament bundle. Error bars correspond to a confidence interval of one standard deviation evaluated over 200 shots.

Assuming that the peak energy deposition is reached mostly due to ionization of O_2 molecules [1], the peak lineic deposited energy is given by:

$$\left.\frac{\partial \Delta U}{\partial z}\right|_{max} = \int_{\mathbb{R}^2} n_{e,max}(r, z_{max}) U_{O_2} r \, \mathrm{d}r\mathrm{d}\theta \approx n_{e,max}(z_{max}) U_{O_2} \pi r_0^2, \tag{6}$$

where $U_{O_2} \approx 12$ eV is the ionization potential of O_2, z_{max} the position along the multifilament bundle where the peak lineic energy deposition is reached and r_0 the HWHM of the electron density profile. Peak electron density in the case of single filaments generated using a $\sim f/30$ focusing has been recorded [23] and numerically estimated [24] to be on the order of 3×10^{23} m^{-3}. Since *superfilamentation* typically results in a peak electron density one order of magnitude higher than in equivalent single filaments, with an equivalent radius in the focal zone of ~ 300 µm [21], the peak lineic deposited energy is therefore estimated at:

$$\left.\frac{\partial \Delta U}{\partial z}\right|_{max} \sim 15 \text{ mJ}\cdot\text{cm}^{-1}, \tag{7}$$

which is indeed close to the measured peak value.

Energy deposition then seems mainly limited by two different factors: first, electron density that can be reached during pulse propagation and, second, the effective length of the plasma column. Tightening the focusing conditions leads to an overall increase of energy deposition because peak electron density rises faster than filament length decreases. However increasing focusing too much becomes detrimental to energy deposition because electron density becomes locally so high that it defocuses the laser pulse very efficiently, preventing its energy from being absorbed by the medium.

#256836 Received 11 Jan 2016; revised 1 Mar 2016; accepted 2 Mar 2016; published 11 Mar 2016

4. Conclusion

In this Article, we presented results from the study of energy deposition in air in the high energy, multifilamentation regime. Influence of experimental parameters on total energy deposition was first investigated. It was found that deposited energy increases with the laser pulse peak power, both in terms of energy and duration. Influence of pulse duration is important, with slight deviations from the minimum duration yielding a significantly lower energy deposition. Influence of pulse energy depends on whether the beam forms a single or multifilaments. In the first case, energy deposition quickly increases with input energy as more and more energy is channeled through the single structure. In the second case, deposited energy still increases with input energy, but does so at a far lower rate as excess energy is redistributed over many competing filaments. As for focusing conditions, we found that strong focusing yielded a significantly higher energy deposition than weak focusing. However increasing the focusing too much actually leads to a significantly lower energy deposition, due to the strong generated plasma, preventing from efficiently channeling laser energy at the focal point. Optimal focusing was evaluated at $f/30$ for a 165 mJ pulse energy and a 50 fs pulse duration, yielding the deposition of more than 60 % of the input energy.

Filamentation-induced hydrodynamics were then studied by means of transverse interferometry. As the beam propagates in the multifilamentation regime, initial energy deposition takes place in many parallel structures in an inhomogeneous fashion. However in the focal zone, where *superfilaments* occur [21], air structures spontaneously evolve towards a quasi cylindrically symmetrical state after a delay typically on the order of 1 µs. We explain this phenomenon by the constructive interference between individual shock waves generated by each superfilament, and the relatively cylindrical distribution of these superfilaments. Going away from the focal zone, symmetrization due to the shock wave process is only partial but still happens over longer timescales ($\sim$ 100 µs) due to thermal diffusion. This symmetrization process enabled us to use a sonographic analysis to estimate the spatial evolution of the lineic deposited energy. It was found that energy densities above 1 $\mathrm{mJ \cdot cm^{-1}}$ could be reach over 15 cm, with a peak lineic energy of more than 1 $\mathrm{J \cdot m^{-1}}$. These results are particularly interesting in the prospect of filamentation-induced air virtual optical structures, such as virtual waveguides or for enhanced aerodynamics.

#256836 Received 11 Jan 2016; revised 1 Mar 2016; accepted 2 Mar 2016; published 11 Mar 2016